

Vortex fluctuations in underdoped $\text{Bi}_2\text{Sr}_2\text{CaCu}_2\text{O}_{8+\delta}$ crystals

Sylvain Colson,¹ Marcin Konczykowski,¹ Marat B. Gaifullin,² Yuji Matsuda,² Piotr Gierłowski,³ Ming Li,⁴

Peter H. Kes⁴ and Cornelis J. van der Beek,¹

¹*Laboratoire des Solides Irradiés, CNRS-UMR 7642 and CEA/DSM/DRECAM, Ecole Polytechnique, 91128 Palaiseau, France*

²*Institute for Solid State Physics, University of Tokyo, Kashiwanoha, Kashiwa, Chiba 277-8581, Japan*

³*Institute of Physics, Polish Academy of Sciences, Al. Lotników 32/46, 02-668 Warsaw, Poland*

⁴*Kamerlingh Onnes Laboratorium, Leiden University, P.O. Box 9506, 2300 RA Leiden, the Netherlands*

(Dated: November 21, 2018)

Vortex thermal fluctuations in heavily underdoped $\text{Bi}_2\text{Sr}_2\text{CaCu}_2\text{O}_{8+\delta}$ ($T_c=69.4$ K) are studied using Josephson plasma resonance (JPR). From the zero-field data, we obtain the c -axis penetration depth $\lambda_{L,c}(0) = 230 \pm 10$ μm and the anisotropy ratio $\gamma(T)$. The low plasma frequency allows us to study phase correlations over the whole vortex solid state, and to extract a wandering length r_w of vortex pancakes. The temperature dependence of r_w as well as its increase with dc magnetic field is explained by the renormalization of the vortex line tension by the fluctuations, suggesting that this softening is responsible for the dissociation of the vortices at the first order transition.

PACS numbers: 74.60.Ec, 74.40.Jg, 74.60.Ge

Vortex thermal fluctuations are considered essential in determining the (H, T) phase diagram of layered high temperature superconductors (HTS), and notably the first order transition (FOT) in which the ordered vortex crystal transforms to a liquid state without long range phase coherence [1, 2]. Many scenarios, varying from vortex lattice melting described by a Lindemann criterion [3] to layer decoupling [4, 5, 6], all considering various degrees of coupling between the superconducting layers, have successfully been used to describe the position of the FOT in the (H, T) -plane. However, such fits to the FOT line have not been able to convincingly discriminate between the different models. Here, we aim to do just this, through a direct measurement of the amplitude, as well as the field and temperature dependence of vortex thermal excursions in the vortex solid phase (or “Bragg-glass” [7]) that lead to the FOT.

For this study, we use the layered $\text{Bi}_2\text{Sr}_2\text{CaCu}_2\text{O}_{8+\delta}$ (BSCCO) compound, in which vortex excursions can conveniently be measured by the Josephson Plasma Resonance (JPR) technique [8, 9, 10]. Briefly, the interlayer Josephson current $J_m^{(c)}$ can be measured through the JPR frequency $\omega_{pl} \sim J_m^{(c)1/2}$, at which the equality of charging and kinetic energy leads to a collective excitation of Cooper pairs across the layers. In turn, $\omega_{pl}^2(B, T) = \omega_{pl}^2(0, T) \langle \cos(\phi_{n,n+1}) \rangle$ intimately depends on the gauge-invariant phase difference $\phi_{n,n+1}$ between adjacent layers n and $n+1$ [11]. Here, $\langle \dots \rangle$ stands for thermal and disorder averaging. Thus, JPR is a probe of the interlayer phase coherence. The fluctuations of vortex lines created by a dc magnetic field applied perpendicularly to the layers modify the relative phase difference between adjacent layers and thus depress ω_{pl} . In $\text{Bi}_2\text{Sr}_2\text{CaCu}_2\text{O}_{8+\delta}$, the ensemble of vortex lines should be described as stacks of two-dimensional pancake vortices. Thermal fluctuations shift the individual vortex pancakes with respect to their nearest neighbors in the c direction,

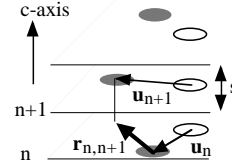


FIG. 1: Meandering of vortex pancakes along the vortex line in layered superconductors. Because of thermal fluctuations and disorder, pancakes (full circles) are shifted away from their equilibrium position (open circles).

by a distance $\mathbf{r}_{n,n+1} = \mathbf{u}_{n+1} - \mathbf{u}_n$. Here \mathbf{u}_n is the ab -plane displacement of the pancake vortex in layer n with respect to the equilibrium position of the stack it belongs to (Fig. 1). The wandering length of vortex lines, which is related directly to the JPR frequency ω_{pl}^2 , can be then defined as $r_w = \langle \mathbf{r}_{n,n+1}^2 \rangle^{1/2}$ [13, 14]. Below, we shall only consider temperatures above $T = 42$ K, at which vortex pinning (quenched disorder) is unimportant [2, 12].

Underdoped BSCCO ($T_c = 69.4$ K) single crystals were grown by the traveling solvent floating zone method in 25 mbar O_2 partial pressure at the FOM-ALMOS center, the Netherlands [15]. The samples were post-annealed for one week at 700°C in flowing N_2 . The advantage of using heavily underdoped BSCCO is that $\omega_{pl}(0, 0) \approx 61$ GHz turns out to be very low, which allows us to measure the vortex meandering over the entire vortex phase diagram. Samples A and B (cut from the same crystal) have dimensions $1.35 \times 1 \times 0.04$ mm^3 and $0.7 \times 0.47 \times 0.04$ mm^3 , respectively. Another sample from the same batch was used to determine the temperature of the FOT (Fig. 5b, inset), by measuring the paramagnetic peak at the FOT with a miniature Hall probe magnetometer [16].

The JPR measurements were carried out using the cavity perturbation technique in the Laboratoire des Solides Irradiés (on sample A) and the bolometric method in

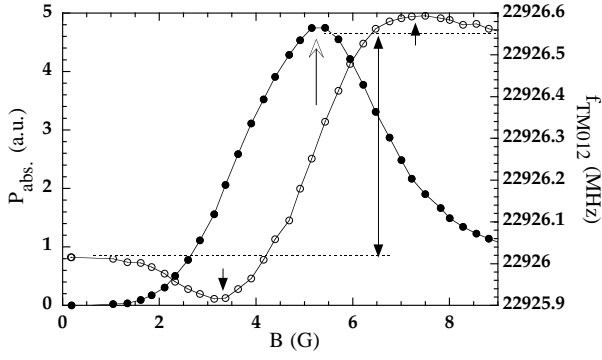


FIG. 2: Field sweep experiment on sample A at $T = 66$ K in the TM_{012} mode of the cavity ($f = 22.9$ GHz). The power absorbed (\bullet , left axis) in the sample shows a maximum at $B_{\text{JPR}} = 5.3$ G at which $\omega = \omega_{\text{pl}}$ (open arrow). At the same field, the resonance frequency of the cavity (\circ , right axis) displays a double-peak structure, indicated by the closed arrows, and a jump (arrow between dashed lines).

the Institute for Solid State Physics at the University of Tokyo (on samples A and B). For the cavity perturbation technique, the sample was glued in the center of the top cover of a cylindrical Cu cavity used in the different TM_{01i} ($i = 0, \dots, 4$) modes. These provide the correct configuration of the microwave field at the sample location, in which $E_{\text{rf}} \parallel c$ -axis and $H_{\text{rf}} \approx 0$ [17]. The unloaded quality factor Q_0 is measured as function of temperature and field to obtain the power absorbed by the sample (Fig. 2). The bolometric method [18] consists in measuring the heating of the sample induced by the absorption of the incident microwave power when the JPR is excited [9, 17]. Furthermore, reversible magnetization measurements were carried out on sample A using a commercial superconducting quantum interference device magnetometer in order to extract the London penetration depth $\lambda_{L,ab}(T)$ for currents in the ab -plane [15].

Figure 3 shows the JPR frequency $f_{\text{JPR}} = \omega_{\text{pl}}/2\pi$ in zero field obtained by the above-mentioned methods on samples A and B. ω_{pl}^2 is proportional to the maximum interlayer Josephson current along the c -axis [11],

$$\omega_{\text{pl}}^2(H, T) = \omega_{\text{pl}}^2(0, T) \langle \cos(\phi_{n,n+1}) \rangle = \frac{2\pi\mu_0 c^2 s}{\epsilon_r \Phi_0} J_m^{(c)}(B, T) \quad (1)$$

where $J_m^{(c)}(B, T) = J_m^{(c)}(0, T) \langle \cos(\phi_{n,n+1}) \rangle$ is the maximum Josephson current, $s = 1.5$ nm is the interlayer spacing, ϵ_r the high-frequency relative dielectric constant and Φ_0 the flux quantum. Using $\omega_{\text{pl}}(0, T) = c/\lambda_{L,c}(T)\sqrt{\epsilon_r}$ and $\epsilon_r = 11.5$ [19], we obtain the London penetration depth for currents along the c -axis, $\lambda_{L,c}(T)$. When divided by the $\lambda_{L,ab}(T)$ -data from reversible magnetization, this yields, without any model assumptions, the anisotropy parameter $\gamma(T) \equiv \lambda_{L,c}(T)/\lambda_{L,ab}(T)$, shown in the Inset to Fig. 3. Typically, at $T = 0.5T_c$, $\lambda_{L,c} \approx 240$ μm and $\lambda_{L,ab} \approx 400$ nm, so that $\gamma \approx 600$,

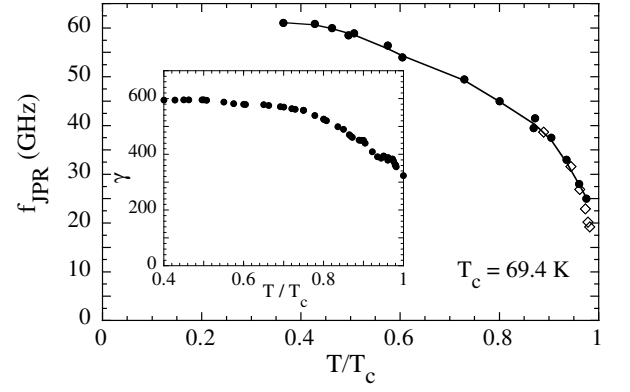


FIG. 3: The JPR frequency in zero magnetic field for samples A (data below 40 GHz) and B (data above 40 GHz) vs the reduced temperature T/T_c . The bolometric method (\bullet) and the cavity perturbation technique (\diamond) have been used. We use a spline fit (solid line) in the extraction of the wandering length (see text). Inset: experimental temperature dependence of γ , obtained by the division of the experimental $\lambda_{L,c}(T)$ data by the $\lambda_{L,ab}(T)$ -data from reversible magnetization.

consistent with other data for the same material [9]. Note that γ decreases as function of temperature.

To analyze our JPR data in non-zero magnetic fields, we should divide $\omega_{\text{pl}}(B, T)$ by the zero-field result depicted in Fig. 3. In the absence of a model that satisfactorily describes $\omega_{\text{pl}}(0, T)$ over the whole temperature range, we resort to a spline fit to the experimental data. Next, we extract the vortex wandering length r_w as follows. In the single vortex regime, at very low fields $B < B_J = \Phi_0/\lambda_J^2$, $B < B_\lambda = \Phi_0/4\pi\lambda_{L,ab}^2$, Bulaevskii and Koshelev derived [13, 14]

$$1 - \frac{\omega_{\text{pl}}^2(B, T)}{\omega_{\text{pl}}^2(0, T)} \approx \frac{\pi B}{2\Phi_0} r_w^2 \ln \frac{\lambda_J}{r_w} \quad (2)$$

where the Josephson length $\lambda_J = \gamma s$. We stress that this relation is meaningful only for small excursions $r_w \leq 0.6\lambda_J$, *i.e.* for $\langle \cos(\phi_{n,n+1}) \rangle = \omega_{\text{pl}}^2(B, T)/\omega_{\text{pl}}^2(0, T) \lesssim 1$. More generally, one expects an increase of $1 - \langle \cos(\phi_{n,n+1}) \rangle$ with r_w up to a plateau for large r_w , as was found in recent simulations of the evolution of $1 - \langle \cos(\phi_{n,n+1}) \rangle$ versus $\langle u \rangle/a_0 \sim r_w/a_0$ for a pancake gas ($a_0 = \sqrt{\Phi_0/B}$ is the intervortex spacing) [20]. The numerical data show that $1 - \langle \cos(\phi_{n,n+1}) \rangle$ is almost quadratic in r_w for $0 \lesssim 1 - \langle \cos(\phi_{n,n+1}) \rangle \lesssim 0.7 - 0.8$, in agreement with Eq. (2), if the weak logarithmic dependence on λ_J/r_w is disregarded. Thus, we use

$$r_w^2 = \frac{2\Phi_0}{\pi B} (1 - \langle \cos(\phi_{n,n+1}) \rangle) \quad (3)$$

to obtain an approximation of the wandering length. Since $r_w = \langle (\mathbf{u}_{n+1} - \mathbf{u}_n)^2 \rangle^{1/2} = [2(u^2 - \langle \mathbf{u}_n \cdot \mathbf{u}_{n+1} \rangle)]^{1/2}$, one has, in the case of completely uncorrelated layers (*e.g.* for a pancake gas), $r_w = \langle 2\mathbf{u}_n^2 \rangle^{1/2} \equiv \sqrt{2}u$. Disregarding the “anticorrelated” situation with $\mathbf{u}_n \cdot \mathbf{u}_{n+1} < 0$,

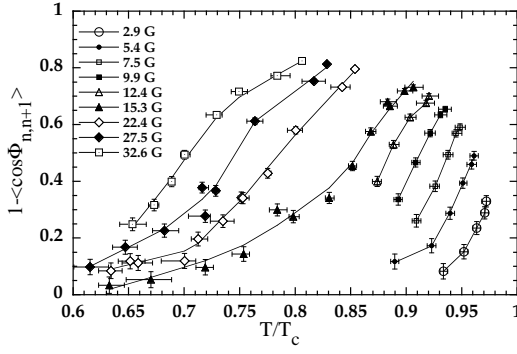


FIG. 4: $1 - \langle \cos(\phi_{n,n+1}) \rangle$ vs temperature for different magnetic fields. We extract r_w from these data using Eq.(3).

correlations between pancake positions in different layers yield $r_w < \sqrt{2}u$, *i.e.*, r_w is a lower limit for the root mean squared (RMS) displacement u of the vortex line.

Figure 4 shows $1 - \omega_{pl}^2(B, T)/\omega_{pl}^2(0, T) = 1 - \langle \cos(\phi_{n,n+1}) \rangle$ as function of temperature in different dc fields. The temperature dependence of the wandering length r_w , obtained by applying Eq. (3), is represented in Fig. 5. For every field, we observe an increase of r_w with T . At constant temperature, r_w increases with magnetic field, indicating a $\omega_{pl}(B)$ -dependence that deviates from the expected linear behavior of Eq. (2). Another interesting feature of the $r_w(T)$ curve is the break in the slope which appears at a field-dependent temperature close to the FOT and above which all the r_w curves merge into one. Alternatively, one may plot the same values of r_w vs T/T_{FOT} , where T_{FOT} is the FOT temperature (Fig. 5b). Here, two regimes appear clearly, showing the correlation of the results with the FOT. For $T < 0.96T_{FOT}$, $r_w(T/T_{FOT})$ roughly overlaps for all fields, whereas for $T > 0.96T_{FOT}$ the curves deviate from each other.

We now discuss the temperature and field dependence of r_w in the vortex solid. The RMS thermal vortex displacement u can be obtained by equipartition of the associated elastic energy with the thermal energy, $U_{el} = c_{44}a_0^2(u^2/s) = k_B T$. The vortex lattice tilt modulus

$$c_{44}(\mathbf{k}) \approx \frac{B^2/\mu_0}{1 + \lambda_c^2 k_{\parallel}^2 + \lambda_{ab}^2 Q_z^2} + \frac{\varepsilon_0}{2\gamma^2 a_0^2} \ln \left[\frac{k_{max}^2}{K_0^2 + (Q_z/\gamma)^2} \right] + \frac{\varepsilon_0}{2\lambda_{ab}^2 Q_z^2 a_0^2} \ln \left(1 + \frac{a_0^2}{21.3 r_w^2} \right), \quad (4)$$

calculated by Koshelev and Vinokur [21] and Goldin and Horowitz [22], consists of three terms: the nonlocal collective (lattice) term, the vortex line tension term, determined by Josephson coupling between layers, and a third term due to the electromagnetic dipole interaction between pancakes. Of particular interest here is the logarithmic correction to the temperature dependence of

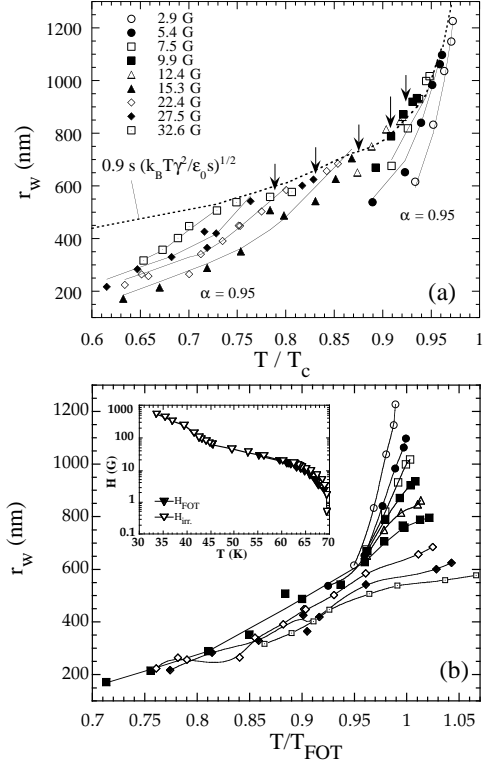


FIG. 5: (a) : Experimental r_w vs T/T_c for different magnetic fields in strongly underdoped BSCCO. For $B = 27.5, 22.4, 15.3, 12.4$ and 9.9 G, arrows show the temperature of the FOT. The dotted line shows the evolution of $0.9s(k_B T \gamma^2 / \varepsilon_0 s)^{1/2}$. Solid lines are fits to Eq. (5) with the single parameter $\alpha = 0.95$, omitting the term $4/\pi (x^2 + 1/4)$ for $B > 15$ G. (b) : r_w vs T/T_{FOT} . Solid lines are guides to the eye. Inset : phase diagram of a sample cut from the same crystal. Full and open triangles stand for the FOT and the irreversibility fields, respectively.

the second term, introduced by the cutoff $k_{max} = \pi/r_w$, which corresponds to the smallest meaningful deformation [21, 22]. To proceed, we evaluate U_{el} at the typical vortex line deformation wavevectors parallel and perpendicular to the layers, $k_{\parallel} \approx \pi/r_w$ and $Q_z \approx \pi\gamma/2a_0 \ll 2\pi/s$. Writing $K_0 = \sqrt{4\pi}/a_0$, $r_w^2 = \alpha u^2$ and $x = a_0/r_w$, equipartition yields

$$r_w^2 \approx \alpha s^2 \frac{k_B T \gamma^2}{\varepsilon_0 s} \left[\frac{4}{\pi (x^2 + 1/4)} + \frac{1}{2} \ln(0.66x^2) + \frac{2}{\pi^2} \left(\frac{a_0}{\lambda_{L,ab}} \right)^2 \ln \left(1 + \frac{x^2}{21.3} \right) \right]^{-1}. \quad (5)$$

All parameters in Eq. (5), and notably $\varepsilon_0(T)/\gamma^2(T) = \Phi_0^2/4\pi\mu_0\lambda_{L,c}^2$, are known from experiment, which allows a direct comparison to the $r_w(T)$ -data. Very good agreement is obtained for the magnitude, the temperature, as well as the field dependence of r_w for the lowest three fields, using the single free parameter $\alpha = 0.95$. For

higher fields, Eq. (5) gives the correct magnitude of r_w , but too weak a temperature dependence. However, excellent fits of both the temperature and field dependence can be obtained for all fields, with the same $\alpha = 0.95$, by omitting the nonlocal collective term, [*i.e.* $4/\pi(x^2 + \frac{1}{4})$ in Eq. (5)], see Fig. 5a. While the main temperature dependence of r_w comes from the prefactor $\gamma^2 T/\varepsilon_0$ in Eq. (5) (dotted line in Fig. 5), the behavior of r_w in the vortex solid can only be understood as the result of the logarithmic correction arising from the softening of the line tension term by thermal fluctuations [21, 22]. The field dependence, originating from Q_z , explicitly indicates that vortex lines are correlated (line-like) on distances that well exceed the layer spacing s .

The experimental data can also be used to compare the terms entering Eq. (4). Deep inside the vortex solid, the line tension always dominates over the magnetic coupling and the nonlocal collective contribution. At very low fields ($B < 10$ G), the line tension term is largest all the way to the FOT. Eq. (5) then reduces to Eq. (40) of Ref. 22 with $Q_z \approx \pi\gamma/2a_0$ instead of $2\pi/s$. At higher fields, the nonlocal collective contribution is expected to increase, eventually exceeding the Josephson coupling (line tension) term close to the FOT (for $B > 20$ G). Nevertheless, the very good fits obtained when *only* the line tension term is taken into account in Eq. (5) suggest that the line tension term always dominates c_{44} near the FOT. Moreover, we find that the electromagnetic coupling as well as the shear contribution to U_{el} are, under all circumstances, negligible. This renders Lindemann-like [3] or dislocation-mediated (Kosterlitz-Thouless like) melting, as well as the vortex-line evaporation [6] scenarios very unlikely. Rather, the large thermal excursions of pancake vortices bring about the softening of the line tension contribution to c_{44} for the large-wavevector modes that lead to the FOT. This would comply with recent measurements showing that vortex lattice order is not a prerequisite for the FOT [23]. For deformations with smaller wavevectors, Josephson coupling still contributes to the line tension even in the vortex liquid, leading to, *e.g.*, the anisotropic vortex response to columnar defects in heavy-ion irradiated samples.

Summarizing, we have carried out JPR measurements on heavily underdoped $\text{Bi}_2\text{Sr}_2\text{CaCu}_2\text{O}_8$ crystals. These data yield the c -axis penetration depth, the anisotropy parameter $\gamma(T)$, and the wandering length of vortex lines r_w . The observed temperature and field dependences of r_w suggest that thermal fluctuations soften the Josephson coupling contribution to the tilt modulus for short wavelengths [22], which leads us to believe that this softening drives the FOT.

We thank the Europe Scientific Foundation VORTEX program and the Nederlandse Organisatie voor Wetenschappelijk Onderzoek for financial support. PG acknowledges support of the Polish Government, grant PBZ-KBN-013/T08/19.

-
- [1] R. Cubitt, E.M. Forgan, G. Yang, S.L. Lee, D. McK. Paul, H.A. Mook, M. Yethiraj, P.H. Kes, T.W. Li, A.A. Menovsky, Z. Tarnawski and K. Mortensen, *Nature* **365**, 410 (1993).
 - [2] E. Zeldov, D. Majer, M. Konczykowski, V.B. Geshkenbein, V.M. Vinokur, and H. Strikman, *Nature* **375**, 373 (1995).
 - [3] G. Blatter, V.B. Geshkenbein, A.I. Larkin, and H. Nordborg, *Phys. Rev. B* **54**, 72 (1996).
 - [4] L. Glazman and A.E. Koshelev, *Phys. Rev. B* **43**, 2835 (1991).
 - [5] L.L. Daemen, L.N. Bulaevskii, M.P. Maley, and J.Y. Coulter, *Phys. Rev. Lett.* **70**, 1167 (1993).
 - [6] M. J. W. Dodgson, A. E. Koshelev, V. B. Geshkenbein and G. Blatter, *Phys. Rev. Lett.* **84**, 2698 (2000).
 - [7] T. Giamarchi and P. Le Doussal, *Phys. Rev. B* **55**, 6577 (1997).
 - [8] O.K.C. Tsui, N.P. Ong, Y. Matsuda, Y.F. Yan, and J.B. Peterson, *Phys. Rev. Lett.* **73**, 724 (1994); Y. Matsuda, M.B. Gaifullin, and K. Kumagai, *ibid.* **75**, 4512 (1995); Y. Matsuda, M. B. Gaifullin, K. Kumagai, M. Kosugi and K. Hirata, *ibid.* **78**, 1972 (1997).
 - [9] M.B. Gaifullin, Yuji Matsuda, N. Chikumoto, J. Shimoyama, and K. Kishio, *Phys. Rev. Lett.* **84**, 2945 (2000).
 - [10] T. Shibauchi, T. Nakano, M. Sato, T. Kisu, N. Kameda, N. Okuda, S. Ooi, and T. Tamegai, *Phys. Rev. Lett.* **83**, 1010 (1999).
 - [11] L. N. Bulaevskii, M. P. Maley, and M. Tachiki, *Phys. Rev. Lett.* **74**, 801 (1995).
 - [12] N. Avraham, B. Khaykovich, Y. Myasoedov, M. Rappaport, H. Shtrikman, D. E. Feldman, T. Tamegai, P. H. Kes, Ming Li, M. Konczykowski, C. J. van der Beek, and E. Zeldov, *Nature (London)* **411**, 451 (2001).
 - [13] L.N. Bulaevskii, A. E. Koshelev, V. M. Vinokur, M. P. Maley, *Phys. Rev. B* **61**, R3819 (2000).
 - [14] A. E. Koshelev and L. N. Bulaevskii, *Physica C* **341-348**, 1503 (2000).
 - [15] Ming Li, C.J. van der Beek, M. Konczykowski, A.A. Menovsky, and P.H. Kes, *Phys. Rev. B* **66**, 024502 (2002).
 - [16] N. Morozov, E. Zeldov, D. Majer, and M. Konczykowski, *Phys. Rev. B* **54**, R3784 (1996).
 - [17] S. Colson, C. J. van der Beek, M. Konczykowski, M. B. Gaifullin, Y. Matsuda, P. Gierlowski, Ming Li, and P. H. Kes, *Physica C* **369**, 236 (2002).
 - [18] Y. Matsuda, N. P. Ong, Y. F. Yan, J. M. Harris, and J. B. Peterson, *Phys. Rev. B* **49**, 4380 (1994).
 - [19] M.B. Gaifullin, Y. Matsuda, N. Chikumoto, J. Shimoyama, K. Kishio, R. Yoshizaki, *Physica C* **362**, 228 (2001).
 - [20] E. H. Brandt and E. B. Sonin, *Phys. Rev. B* **66**, 064505 (2002).
 - [21] A. E. Koshelev and V. M. Vinokur, *Phys. Rev. B* **57**, 8026 (1998).
 - [22] T. R. Goldin and B. Horovitz, *Phys. Rev. B* **58**, 9524 (1998).
 - [23] S.S. Banerjee, A. Soibel, Y. Myasoedov, M. Rappaport, E. Zeldov, M. Menghini, Y. Fasano, F. de la Cruz, C.J. van der Beek, and M. Konczykowski, preprint (2002).